Bragg-induced power oscillations in $\mathcal{PT}$-symmetric periodic photonic structures

P. A. Brandão[*] and S. B. Cavalcanti[†]

Universidade Federal de Alagoas, Cidade Universitária, Maceió-AL, 57072-970, Brazil

We study Bragg-induced power oscillations in Fourier space between a pair of optical resonant transverse modes propagating through a periodic $\mathcal{PT}$-symmetric lattice, represented by a refractive index that includes gain and loss in a balanced way. Our results imply that the $\mathcal{PT}$-symmetric system shows exceptionally rich phenomena absent in its Hermitian counterpart. It is demonstrated that the resonant modes exhibit unique characteristics, such as Bragg power oscillations controlled via the $\mathcal{PT}$ symmetry, severe asymmetry in mode dynamics, and trapped enhanced transmission. We have also performed numerical simulations in (1+1) and (2+1) dimensions of propagating Gaussian beams to compare with analytical calculations developed under a two-waves model.

I. INTRODUCTION

More than a decade ago, a very interesting idea has been put forward by Bender and co-workers on the existence of non-Hermitian Hamiltonians exhibiting a real-valued energy spectrum below a symmetry-breaking point at which the spectrum undergoes a phase transition to the complex plane [1–5]. These non-Hermitian Hamiltonians are very useful for modeling optical systems with a controlled balance between amplification and attenuation, meaning that the refractive index obeys the property $n(x) = n(-x)^*$. Therefore the $\mathcal{PT}$ symmetry concept was soon extended to optical systems by identifying the real part of the potential with the refractive index of the lattice and the imaginary one with gain or loss [6,7]. Complex potentials have received then, in recent years, enormous attention considering the development of these new artificial structures where one may tailor the refractive index according to one's need. Theoretical work based on the paraxial approximation has reported results on the propagation of light beams transversely to an optical lattice that indicate that the input beam power is not conserved along propagation [8]. Experimental work based on $\mathcal{PT}$ Hamiltonians has been suggested in optical media with a complex refractive index [9–12], and $\mathcal{PT}$ symmetry breaking has been firstly reported in experiments based on a passive optical coupler [13]. Bloch oscillations have been proposed [14] and demonstrated in $\mathcal{PT}$-symmetric photonic lattices [15], exhibiting rich phenomena not present in conservative systems. Also, experimental reports on light transport in $\mathcal{PT}$-symmetric temporal lattices have demonstrated that such symmetric periodic structures might act as unidirectional invisible media near a spectral singularity [16]. Spectral singularities are resonant energy eigenvalues that represent states characterized by infinite reflection and transmission coefficients. Spontaneous $\mathcal{PT}$ symmetry breaking and nonreciprocal power oscillations have been observed in a study on the behavior of a $\mathcal{PT}$ optical coupled system [17]. Overall, one may conclude that the applications of $\mathcal{PT}$ symmetry to optical systems should provide new ways to control light propagation, unraveling a world of remarkable

effects with tremendous impact on optical materials, devices, and networks [18].

Motivated by these exciting reports, in this work we wish to investigate the role of $\mathcal{PT}$ symmetry on optical power oscillations, due to the propagation of wide optical beams in complex periodic lattices, whereby the coupling between the beam and the periodic structure results in Bragg-induced power oscillations between transverse modes related by the Bragg resonance condition [19,20]. More specifically, we wish to investigate the consequences of extending the model presented in [19] to the complex domain. It is well known that by doing this, one opens up the way to strange and fascinating properties, particularly on the verge of spectral singularities. In this case, a close examination of Bragg scattering processes has demonstrated that spectral singularities are associated with the secular growth of plane waves that satisfy the Bragg condition and also that they occur at the $\mathcal{PT}$ symmetry-breaking point. Furthermore, it has been reported that, in contrast with wide beams, a wave packet with a broad momentum distribution leads to a saturation of the secular growth of scattered waves [21,22]. In the following we choose a $\mathcal{PT}$ potential periodic function to investigate the influence of $\mathcal{PT}$ symmetry on the behavior of Bragg-induced power oscillations between a pair of Bragg-resonant modes excited by wide optical beams. Based on the two-waves model complemented by numerical simulations of the wave equation by using a Gaussian beam input, we investigate the Bragg-resonant mode behavior below and above the phase transition point, and we obtain all the peculiar universal features of non-Hermitian Hamiltonians, such as nonreciprocal behavior of the Bragg modes, power oscillations, and secular growth of plane waves. Furthermore, we find additional features on the spectral behavior, such as mode trapping and asymmetric mode power transfer.

II. TWO-WAVES MODEL

It is well known that a plane-wave input in general may excite many resonant lattice modes. Here, we suppose that the input power mode is Bragg resonant with the lattice so that the incident plane wave excites mainly the two modes at the edges of the Brillouin zone and ignore all other resonant modes [23]. More specifically, we consider a one-dimensional periodic $\mathcal{PT}$-symmetric potential $V(x)$ function through which a wide beam $\psi(x,z)$ propagates. The propagation dynamics is then

---

[*]paulocabf@gmail.com
[†]sbessa@gmail.com

053841-1

described by the dimensionless paraxial wave equation

$$i\frac{\partial \psi}{\partial z} + \frac{\partial^2 \psi}{\partial x^2} - V(x)\psi = 0, \tag{1}$$

in arbitrary units. Let us define a potential function of the form $V(x) = \alpha[\cos^2 x + i\beta \sin(2x)]$, with α, β representing real parameters (with β positive). It is easy to verify that the so-defined potential satisfies $V(-x)^* = V(x)$, and there is a gain-loss parameter β that controls the degree of Hermiticity. This parameter defines a spontaneous symmetry-breaking point, $\beta_c = 1/2$, above which the spectrum undergoes a phase transition from the real to the complex plane. More specifically, the spectrum is real for $\beta < \beta_c$ and becomes partially or completely complex for $\beta > \beta_c$ [10]. We solve the wave equation by writing the field as

$$\psi(x,z) = \sum_{n=\pm 1,\pm 2...} \psi_n(z) \exp(ink_b x), \tag{2}$$

where $k_b = 1$ is the resonant transverse wave vector and the index n indicates the nth mode that is Bragg resonant with the lattice. Substituting (2) into (1), one arrives at the following set of coupled differential equations:

$$i\frac{d\psi_n}{dz} = a_n\psi_n + b\psi_{n-2} + c\psi_{n+2} \tag{3}$$

with

$$a_n = \left(n^2 + \frac{\alpha}{2}\right) \tag{4}$$

and

$$b = \frac{\alpha}{2}(\beta_c + \beta), \tag{5}$$

$$c = \frac{\alpha}{2}(\beta_c - \beta). \tag{6}$$

Here we study the particular case where $n = \pm 1$ only. This is the essence of the two-waves model, and it was shown to give reliable results when the incident angle is coupled to the edge of the first Brillouin zone [19]. Its validity will be further discussed in Sec. V. Equation (3) is first order in z so that the initial values $\psi_{-1}(0)$ and $\psi_1(0)$ must be specified for a unique solution. To acquire a complete picture of the dynamics, we now consider the following second-order linear differential equation for ψ_{-1}:

$$\frac{d^2\psi_{-1}}{dz^2} + 2ia\frac{d\psi_{-1}}{dz} + (cb - a^2)\psi_{-1} = 0, \tag{7}$$

where $a = a_{-1} = a_1$. Equation (7) is derived from the system of equations (3) for $n = \pm 1$ and considering $\psi_{-3} = \psi_3 = 0$. The equation satisfied by $\psi_1(z)$ is obtained from (7) by performing the operation $\psi_{-1} \to \psi_1$. The general solutions for the modal amplitudes $\psi_{-1}(z)$ and $\psi_1(z)$ are given by

$$\begin{Bmatrix} \psi_{-1}(z) \\ \psi_1(z) \end{Bmatrix} = \frac{1}{2}\left[\begin{Bmatrix} \psi_{-1}(0) \\ \psi_1(0) \end{Bmatrix} - i\begin{Bmatrix} \gamma\psi_1(0) \\ \gamma'\psi_{-1}(0) \end{Bmatrix}\right] \times \exp\left[-\left(\frac{\alpha}{2}+1\right)iz + \frac{|\alpha|}{2}kz\right]$$
$$+ \frac{1}{2}\left[\begin{Bmatrix} \psi_{-1}(0) \\ \psi_1(0) \end{Bmatrix} + i\begin{Bmatrix} \gamma\psi_1(0) \\ \gamma'\psi_{-1}(0) \end{Bmatrix}\right] \times \exp\left[-\left(\frac{\alpha}{2}+1\right)iz - \frac{|\alpha|}{2}kz\right], \tag{8}$$

where

$$\gamma = \text{sgn}(\alpha)\frac{(\beta - \beta_c)}{k}, \tag{9}$$

$$\gamma' = \text{sgn}(\alpha)\frac{(\beta + \beta_c)}{k}, \tag{10}$$

$k = \sqrt{\beta^2 - \beta_c^2}$, and $\text{sgn}(\alpha)$ is $+1$ or -1 depending on the sign of α. The initial conditions $\{\psi_{-1}(0), \psi_1(0)\}$ together with relations (8), (9), and (10) determine the system's evolution. Before we discuss some more involved peculiarities, note the apparent asymmetry in the evolution of the two modal functions that is solely due to the γ and γ' terms. This parameter may be either real or complex depending on the system being below ($\beta < \beta_c$) or above ($\beta > \beta_c$) the critical phase point. To fully grasp the system's dynamics, in the following we separate the discussion in these two cases.

Before we proceed, it is useful to define the population inversion function $W(z)$ which characterizes the spectral energy exchange between the two resonant modes. We define $W(z) = |\psi_1(z)|^2 - |\psi_{-1}(z)|^2$, representing the difference in power spectra of the two modes. A $\mathcal{PT}$-symmetric system, in general, does not satisfy symmetric initial conditions and thus one must distinguish two cases depending on the values of

$\psi_{-1}(0)$ and $\psi_1(0)$. Let us begin by choosing $\{\psi_{-1}(0), \psi_1(0)\} = \{1,0\}$, so that,

$$W_{-1} = \tfrac{1}{4}[(|\gamma'|^2 - 1)e^{-(k+k^*)z} - (1+|\gamma'|^2)e^{-(k-k^*)z}$$
$$-(1+|\gamma'|^2)e^{(k-k^*)z} + (|\gamma'|^2 - 1)e^{(k+k^*)z}]. \tag{11}$$

On the other hand, by choosing $\{\psi_{-1}(0), \psi_1(0)\} = \{0,1\}$, the population inversion becomes

$$W_1 = \tfrac{1}{4}[(1 - |\gamma|^2)e^{-(k+k^*)z} + (|\gamma|^2 + 1)e^{-(k-k^*)z}$$
$$+(|\gamma|^2 + 1)e^{(k-k^*)z} + (1 - |\gamma|^2)e^{(k+k^*)z}]. \tag{12}$$

These expressions form the basis for the discussion of population inversion in systems with $\mathcal{PT}$ symmetry within the two-waves approach and will be used extensively in the next sections.

III. POPULATION INVERSION BELOW THE PHASE TRANSITION POINT

In the case $0 \leqslant \beta \leqslant \beta_c$ one may define $k = i\kappa$ with $\kappa = \sqrt{\beta_c^2 - \beta^2} \geqslant 0$, a real non-negative constant. Let us first consider a real lattice for which $\beta = 0$. Then, $|\gamma|^2 = |\gamma'|^{-2} = 1$, $k = i\beta_c$ and Eqs. (11) and (12) give $W_{-1} = -\cos(|\alpha|z/2)$
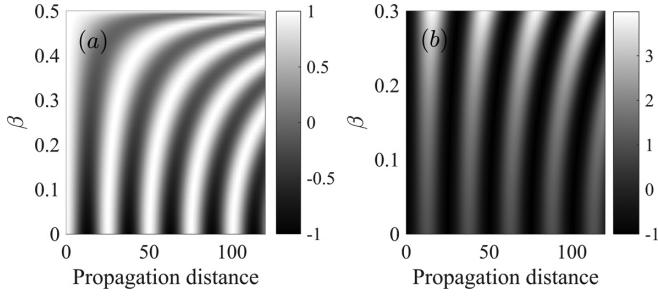
FIG. 1. (a) Population inversion W_1 in a $\mathcal{PT}$-symmetric lattice as a function of the order parameter β and propagation distance for $\beta < \beta_c$, illustrating power oscillations. (b) The same for W_{-1} with β chosen to be in the range $[0,0.3]$ to make the color scale easier for visualization. Notice how the color scale goes beyond the value of 1. For this picture we have assumed $\alpha = 0.5$.

and $W_1 = \cos(|\alpha|z/2) = -W_{-1}$, which are symmetric so that the system executes full power spectra oscillations with a complete periodic transfer of energy between the two modes at every multiple of $z_p = 4\pi/|\alpha|$ [19]. Things become very different for a complex lattice. To illustrate how the population inversion evolves in this scenario, we choose $0 \leqslant \beta \leqslant \beta_c$, so that Eqs. (11) and (12) become

$$W_1 = \cos^2\left(\frac{|\alpha|\kappa z}{2}\right) - \frac{(\beta_c - \beta)}{(\beta_c + \beta)}\sin^2\left(\frac{|\alpha|\kappa z}{2}\right), \quad (13)$$

$$W_{-1} = -\cos^2\left(\frac{|\alpha|\kappa z}{2}\right) + \frac{(\beta_c + \beta)}{(\beta_c - \beta)}\sin^2\left(\frac{|\alpha|\kappa z}{2}\right), \quad (14)$$

which clearly highlights the asymmetry of the system due to the factors γ and γ'. The two-parameter families of functions $W_{-1}(\beta,z)$ and $W_1(\beta,z)$ may be visualized in color plots to illustrate power spectra oscillations when the lattice is below the phase transition point. Let us turn to Fig. 1, where W_1 and W_{-1} are respectively plotted in Figs. 1(a) and 1(b), from which many interesting conclusions are drawn. Figure 1(a) shows that if $\beta \approx 0$, one retrieves the conservative power oscillation as a function of propagation distance, here described by $W_1 \approx \cos(|\alpha|z/2)$, with colors ranging from $+1$ (white) to -1 (black) for all z. This means that power oscillations are represented here by the successive regions of white and black, in the sense that power is more present in mode ψ_1 in white regions and is more present in mode ψ_{-1} in dark ones. Therefore in Fig. 1 white regions mean more power within mode ψ_1 and dark regions mean more power within mode ψ_{-1}. Gray regions mean that the power is shared between the two modes in Fig. 1(a). On the other hand, Fig. 1(b) shows that if the initial power spectrum is in the mode ψ_{-1}, oscillations are retrieved, although the spectra amplitudes are much larger in mode ψ_1 than the previous case, indicating that power transfer is much more efficient to mode ψ_1 than to mode ψ_{-1} (see also Fig. 2). As β approaches the critical value β_c, there is a distortion of the vertical lines in Fig. 1, that is mainly due to the term $\sqrt{\beta_c^2 - \beta^2}$ inside the trigonometric functions in Eqs. (13) and (14). To see more clearly what is actually happening at the critical point, let us substitute $\beta = \beta_c$ directly in Eq. (13) to obtain

$$W_1(z) = 1. \quad (15)$$
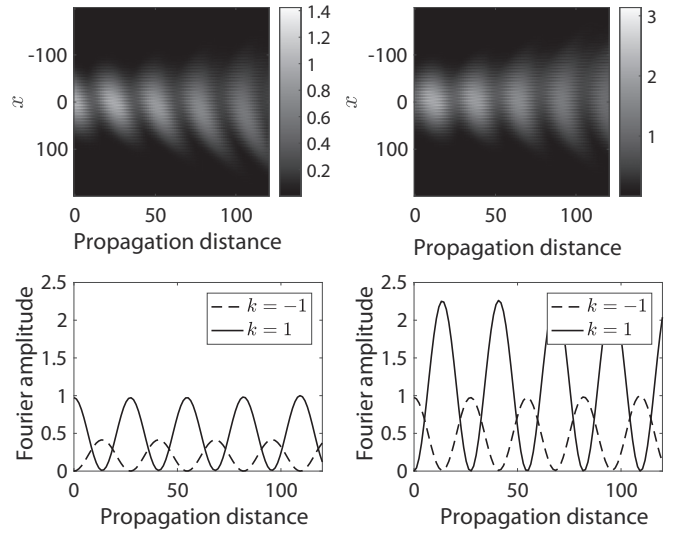
FIG. 2. Gaussian beam propagation below the phase transition point ($\beta < \beta_c$) in both real (upper panels) and Fourier spaces (lower panels), illustrating power oscillations with $\beta = 0.2$ and $\alpha = 0.5$. Left column: $\{\psi_{-1}(0),\psi_1(0)\} = \{0,1\}$. Right column: $\{\psi_{-1}(0),\psi_1(0)\} = \{1,0\}$. Excited modes outside the first Brillouin zone are indistinguishable from the horizontal zero axis line.

Exactly at the transition point, when the input power is located initially in mode ψ_1, it will remain trapped in this mode forever independent of the propagation distance. There is a perfect balance of energy exchange between lattice and wave field such that a stable intensity evolution is achieved. When β is smaller than β_c, power oscillations are modulated, through the $\mathcal{PT}$ symmetry of the lattice, with an increase in the oscillation period. This behavior is evident by a close inspection of Fig. 1 and also by Eq. (13), where β appears inside the sine (cosine) and thus controls the oscillation period together with the value of $|\alpha|$. On the other hand, when the initial state of the system is defined by $\{\psi_{-1}(0),\psi_1(0)\} = \{1,0\}$, the parameter γ' suggests some peculiar behavior and, by taking the limit $\beta \rightarrow \beta_c$ directly, as was done earlier, we obtain from (14)

$$W_{-1} = -1 + \frac{|\alpha|^2}{4}z^2, \quad (16)$$

where we used the fact that $\lim_{p\rightarrow 0} \sin^2(\sqrt{p}y)/p = y^2$. The population difference exhibits secular growth during propagation when $\beta = \beta_c$ exactly. This means that the lattice is transferring energy preferably to mode $\psi_1(z)$, because W_{-1} will certainly become positive. To better visualize this, one may write the total field (2) at $\beta = \beta_c$ [with $\{\psi_{-1}(0),\psi_1(0)\} = \{1,0\}$],

$$\psi(x,z) = e^{-i(1+\alpha/2)z}\left[\mathrm{sgn}(\alpha)\frac{\alpha z}{2i}e^{ix} + e^{-ix}\right], \quad (17)$$

where it is easy to see that, indeed, the first amplitude factor, which is responsible for the mode $\psi_1(z)$, grows linearly with the propagation distance, while the mode at $k = -1$ remains constant.

Next, we compare numerical results based on the propagation of a wide Gaussian beam input with spatial spectral power centered at the edge of the Brillouin zone, with the
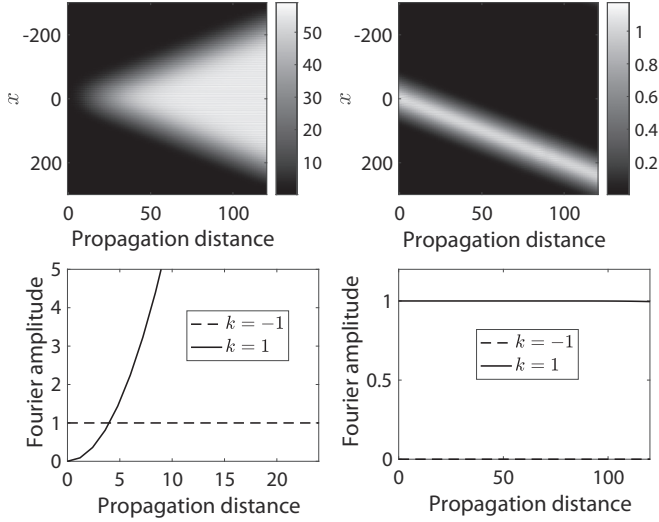
FIG. 3. Wide Gaussian beam propagation at the critical phase point $(\beta = \beta_c)$ in both real (upper panels) and Fourier (lower panels) spaces, with initial width $X_0 = 15p$ (p is the lattice period) incident on a $\mathcal{PT}$-symmetric lattice at the critical point. Left column: $\{\psi_{-1}(0), \psi_1(0)\} = \{1, 0\}$. Right column: $\{\psi_{-1}(0), \psi_1(0)\} = \{0, 1\}$. Excited modes outside the first Brillouin zone are indistinguishable from the zero horizontal axis line.

analytic ones obtained from the two-waves model. To this end we solve Eq. (1) using a split-step Fourier method with a Strang splitting, with the input

$$\psi(x, 0) = \exp\left[-\frac{1}{2}\left(\frac{x}{X_0}\right)^2\right] \exp(\pm ix), \qquad (18)$$

$\alpha = 0.5$, and initial width $X_0 = 15p$, where p is the lattice period. Power oscillations are illustrated in Fig. 2, where the propagation of a Gaussian beam in both real (upper panels) and Fourier (lower panels) spaces is shown, below the transition point, whether the initial condition is $\{\psi_{-1}(0), \psi_1(0)\} = \{0, 1\}$ or $\{\psi_{-1}(0), \psi_1(0)\} = \{1, 0\}$, presented in the left and right panels, respectively. The asymmetry regarding the transfer of power spectra between the two modes is clearly evident by inspecting the Fourier amplitudes. Note the striking contrast between the dynamics in these two cases. The initial Fourier spectrum is centered at $k_i = -1$ (left panels) or at $k_i = 1$ (right panels). Excited modes outside the first Brillouin zone, at $k = \pm 3$ and beyond, are indistinguishable from the horizontal zero axis line (not shown). Figure 3 shows the numerical result of the Gaussian beam propagation in both real (upper panels) and reciprocal (lower panels) spaces, with $\beta = \beta_c$. When $\{\psi_{-1}(0), \psi_1(0)\} = \{0, 1\}$ (right panels), one may clearly see that the initial Gaussian beam propagates along a definite angle with a steady intensity. This result is in good agreement with the analytic result predicted by Eq. (15). On the other hand, the initial condition $\{\psi_{-1}(0), \psi_1(0)\} = \{1, 0\}$ (left panels) indicates that in this case, the lattice is giving energy to the field and, as a result, the intensity increases indefinitely during propagation. Notice the dominance of the $\psi_1(z)$ mode, no matter where the input is; energy always flows higher to this mode. Figure 4 shows the intensity as a function of the propagation distance at $x = 0$. Due to the previous
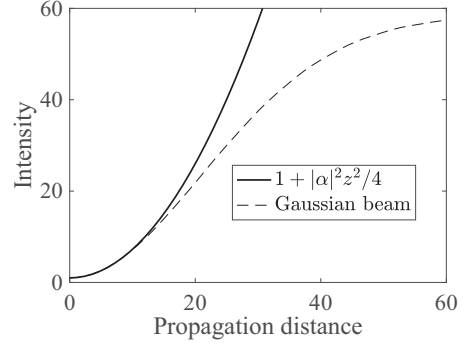
FIG. 4. Intensity at $x = 0$ as a function of the propagation distance with the lattice at the critical point. The dashed line represents the intensity obtained from the simulation with a Gaussian beam. Continuous line is the analytic result from the two-waves model [Eq. (17)]. For this simulation we have assumed $\alpha = 0.5$.

analysis, one expects that the intensity evolves according with $|\psi(0, z)|^2 = 1 + (|\alpha|z)^2/4$, and we compare this evolution, in long propagation distances predicted by the two-waves model (solid line), with the evolution of a Gaussian beam (dashed line). We find that in this case the contribution of other modes apart from the two considered here indicates a tendency to the spectral broadened induced saturation effect that is known to neutralize secular growth reported in [21] (dashed line in Fig. 4). Nevertheless, the initial overall behavior before the saturation effect takes place, and the role of the $\mathcal{PT}$-symmetric lattice, are clearly captured by the two-waves model.

IV. POPULATION INVERSION ABOVE THE PHASE TRANSITION POINT

When $\beta \geqslant \beta_c$ the system has undergone a phase transition, meaning that eigenvalues of the Hamiltonian operator in Eq. (1) have become complex or partially complex. This has a tremendous consequence on the population inversion described by Eqs. (11) and (12), which now reads

$$W_{-1} = -\cosh^2\left(\frac{|\alpha|kz}{2}\right) + \frac{(\beta + \beta_c)}{(\beta - \beta_c)} \sinh^2\left(\frac{|\alpha|kz}{2}\right), \quad (19)$$

$$W_1 = \cosh^2\left(\frac{|\alpha|kz}{2}\right) - \frac{(\beta - \beta_c)}{(\beta + \beta_c)} \sinh^2\left(\frac{|\alpha|kz}{2}\right), \quad (20)$$

clearly displaying uncontrolled diverging behaviors. After a close inspection of Eqs. (19) and (20), one concludes that the energy-transfer process is not symmetric with respect to the excited modes in the sense that the energy flow is always directed towards $\psi_1(z)$, no matter the initial condition one chooses. This asymmetric mode evolution is typical of $\mathcal{PT}$-symmetric Hamiltonians. In Fig. 5 we illustrate this statement by plotting W_{-1} (dashed line) and W_1 (solid line) for $\beta = 1$ and $\alpha = 0.5$ as functions of the propagation distance z. The asymmetry in the dynamics of the pair is evident in view of a privileged mode, namely, ψ_1, for which power always flows whether the initial state is populated or not.

Let us now compare the field intensity evolution of the analytic approach with the Gaussian beam, as we did in the previous section. By considering $\{\psi_{-1}(0), \psi_1(0)\} = \{0, 1\}$, it is
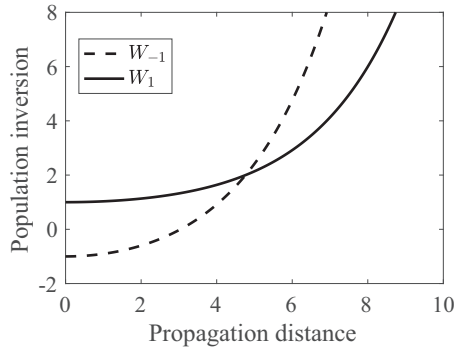
FIG. 5. Population inversion for a system above the phase transition point as a function of the propagation distance z with with $\beta = 1$ and $\alpha = 0.5$. Dashed line: W_{-1}. Solid line: W_1. Clearly, the lattice energy flows towards mode $\psi_1(z)$ are dominant.

straightforward to show that

$$|\psi(0,z)|^2 = \frac{\beta}{\beta + \beta_c} \cosh\left(|\alpha|\sqrt{\beta^2 - \beta_c^2}z\right) + \frac{\beta_c}{\beta + \beta_c},$$
(21)

which means that above the phase transition point, the model predicts an exponential growth for the intensity, controlled by the hyperbolic cosine function. Figure 6 depicts the field evolution predicted by (21) compared with a Gaussian initial condition. Thus one may conclude that the lattice is giving energy to the field during propagation and that this energy transfer is even more pronounced when the system is above the phase transition point.

V. THE TWO-WAVES APPROXIMATION

One of the main reasons for the contrasting behavior exhibited in Figs. 4 and 6 stems from the fact that the two-waves approximation implies a shallow potential function, for it determines the lattice coupling strength with other beam modes, besides the pair considered. This strength is represented here by the overall amplitude coefficient α, that we have assumed equal to 0.5 in the previous discussed results. At
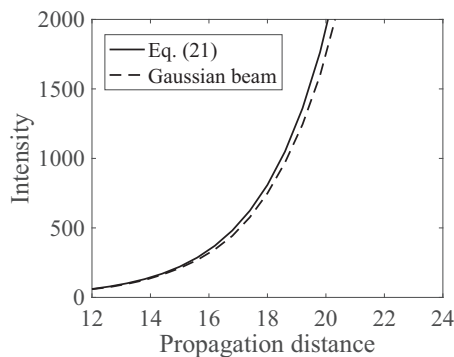
FIG. 6. Field intensity evolution at $x = 0$ of a wave field during propagation above the phase transition point with the same parameters as Fig. 5. The dashed line represents the intensity from the numerical simulation with a Gaussian beam. The solid line is obtained from the two-waves approach.
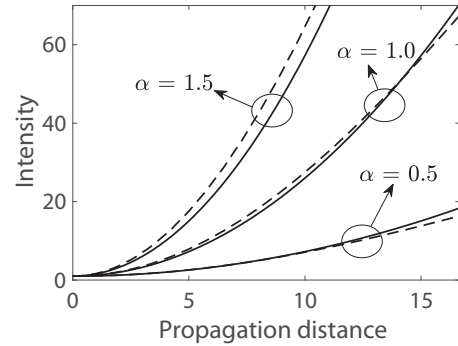
FIG. 7. (Dashed lines) Gaussian beam intensity evolution at $x = 0$ as a function of the propagation distance for three values of α. (Solid lines) Corresponding two-mode approach $1 + (|\alpha|z/2)^2$.

the symmetry-breaking point, $\beta = \beta_c$, the intensity at $x = 0$ is obtained from Eq. (17):

$$|\psi(0,z)|^2 = 1 + \frac{|\alpha|z^2}{4}.$$
(22)

So, the parameter α represents a correction to the parabolic curvature of the intensity. This result is illustrated in Fig. 7, where the evolution of the intensity at $x = 0$ of a Gaussian input with the propagation distance is shown for three values of α. It is clear that as long as $|\alpha| \lesssim 1$, the analytic model reaches a better agreement with more realistic beam sources for a determined propagation distance. This is expected because the propagating beam excites few modes for $|\alpha| \ll 1$. In contrast, larger values of α lead to the coupling with other modes. To see the coupling effect promoted by α, we have plotted in Fig. 8 the spectrum power correspondent to the intensity shown in Fig. 7 for $z = 15$, where the appearance of another mode at $k_b = 3$ is clear. For this graph we have normalized the maximum value of the Fourier modes so that the maximum value of the mode seen at $k_b = 1$ is 1. Note that increasing the absolute value of α leads to the enhancement in the amplitude of the additional Fourier mode and the mode at $k_b = 2$ is
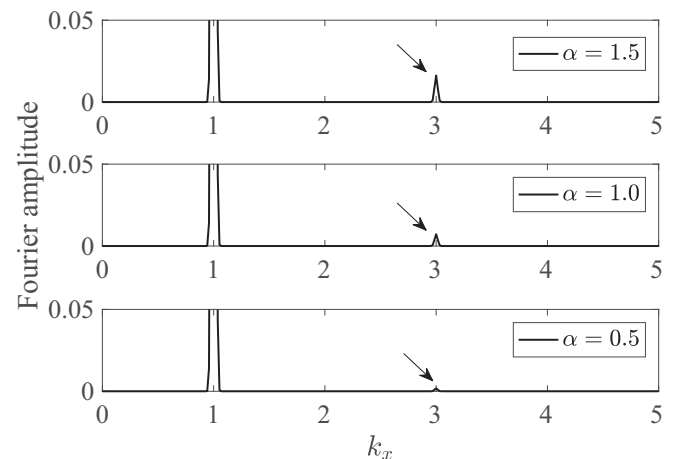
FIG. 8. Fourier amplitudes correspondent to the intensity depicted in Fig. 7 for the same values of α at $z = 15$. The plot is normalized such that the maximum value of the Fourier amplitude at $k_x = 1$ is 1.
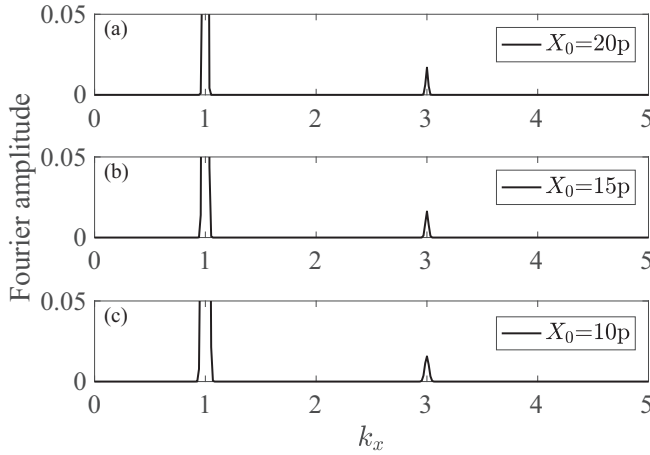
FIG. 9. Fourier amplitude with fixed $\alpha = 1.5$ and various input beam widths [Fig. 8(a)] and (a) $X_0 = 20p$, (b) $X_0 = 15p$, and (c) $X_0 = 10p$. The plot is normalized such that the maximum value of the Fourier amplitude at $k_x = 1$ is 1.

not excited at all for the lattice couples with odd integers only, $\pm 1, \pm 3$, etc. [see Eq. (3)]. The coupling effect is also apparent in Fig. 9, where the Fourier amplitudes corresponding to Fig. 8(a), i.e., for fixed $\alpha = 1.5$ and $z = 15$, and various beam widths are depicted. Here, it should be noted that the only effect promoted by narrow input beams is to broaden the resonant Fourier amplitudes. However, their amplitudes keep still, as the maximum value of their Fourier amplitude is not modified. Particularly, the additional mode at $k_b = 3$ becomes wider but not higher, and so one might conjecture that this fact could be the reason why the analytic approach yields such reliable results. More specifically, it suggests that secondary modes are less efficiently excited due to the spectral broadening. In this way one concludes that this maximum is determined solely by the value of α and that efficient coupling is determined fundamentally by the potential strength. This result is quite reasonable by having in mind that a finite input beam, in spite of providing additional modes to be excited, does not promote the coupling, which is not going to happen when the potential is too weak to induce secondary expressive scattering processes. Therefore, the two-waves model, in spite of its simplicity, describes quite well the overall behavior of light propagation in a complex lattice in the case of shallow potential functions and multimode optical fields.

VI. SPECTRAL POWER OSCILLATIONS IN (2+1) DIMENSIONS

Let us now find whether our analysis can still give reasonable results when extended to higher dimensions. To this end, in the following we wish to investigate the mode-trapping effect at the symmetry-breaking point, observed above, considering a propagating two-dimensional (2+1) optical field $\psi(x,y,z)$. We then write the two-dimensional version of Eq. (1),

$$i\frac{\partial \psi}{\partial z} + \frac{\partial^2 \psi}{\partial x^2} + \frac{\partial^2 \psi}{\partial y^2} - V(x,y)\psi = 0, \quad (23)$$
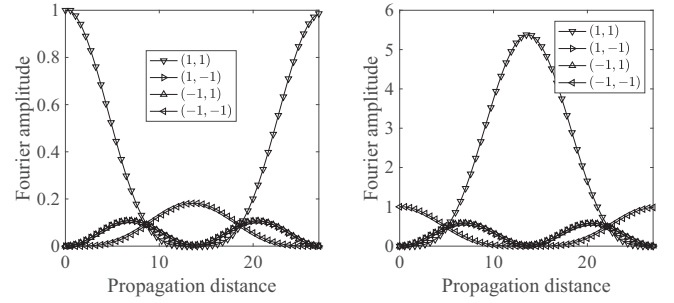
FIG. 10. Bragg-induced power oscillations in two-dimensional beams with the lattice below the symmetry-breaking point for $\alpha = 0.5$ and $\beta = 0.2$. Evolution of the Fourier amplitudes when the Fourier spectrum of the incident beam is located at (left) $(k_{bx}, k_{by}) = (1,1)$ and (right) $(k_{bx}, k_{by}) = (-1,-1)$. This plot is normalized such that the initial Fourier amplitude in both cases is equal to unity.

with the $\mathcal{PT}$-symmetric potential [10]

$$V = \alpha\{\cos^2 x + \cos^2 y + i\beta[\sin(2x) + \sin(2y)]\}. \quad (24)$$

In a two-dimensional system there are four modes in the first Brillouin zone that are effective coupled so that in 2D systems, one must use the four-waves model instead. By expanding the field according to Eq. (2),

$$\psi(x,y,z) = \sum_{n,m=\pm 1, \pm 2, \ldots} \psi_{n,m}(z)e^{inx+imy}, \quad (25)$$

and inserting Eq. (25) into Eq. (23) one obtains the following coupled linear differential equation for the modes $\psi_{n,m}(z)$:

$$i\frac{d\psi_{n,m}}{dz} = a\psi_{n,m} + b(\psi_{n-2,m} + \psi_{n,m-2})$$
$$+ c(\psi_{n+2,m} + \psi_{n,m+2}) = 0, \quad (26)$$

where $a = (n^2 + m^2 + \alpha)$, and b and c are given by (5) and (6), respectively. Although analytic solutions to this more general case are still possible, they are quite cumbersome and, therefore, we attempt to solve Eq. (23) numerically with a Gaussian initial condition to verify the mode-trapping phenomenon at the symmetry-breaking point. More specifically, we suppose that the coupling is effective only at the corners of the first Brillouin zone, so that the initial Gaussian beam amplitude, $\psi(x,y,0)$, may be written as

$$\psi(x,y,0) = \exp\left[-\frac{(x^2+y^2)}{2X_0^2}\right]\exp(ik_{bx}x + ik_{by}y), \quad (27)$$

where $X_0 = 8p$ is the beam width and (k_{bx}, k_{by}) are the components of the incident Fourier components. But first, let us study the two-dimensional analog of Fig. 2. To this end, we assume $\alpha = 0.5$, $\beta = 0.2$ and the initial condition described by Eq. (27). The Fourier amplitudes evolution for the particular inputs centered at $(k_x, k_y) = (\pm 1, \pm 1)$ are depicted in Fig. 10 as the propagation distance z increases. We clearly note the typical $\mathcal{PT}$ asymmetry also present in the one-dimensional counterpart. In Fig. 11 we plot the same Fourier amplitudes as in Fig. 10 but with the lattice at the symmetry-breaking point $\beta = \beta_c = 0.5$. On the right part of this figure, one can see that the lattice still supplies the field with optical energy. The left part of Fig. 11, however, indicates that the
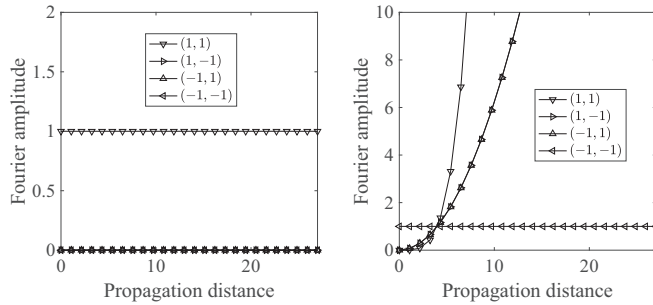
FIG. 11. Two-dimensional mode trapping in a $\mathcal{PT}$-symmetric lattice for $\alpha = 0.5$ and $\beta = 0.5$. The Fourier amplitude of the incident beam is located at (left) $(k_{bx}, k_{by}) = (1, 1)$ and (right) $(k_{bx}, k_{by}) = (-1, -1)$. This plot is normalized such that the initial Fourier amplitude in both cases is equal to unity.

initial mode located at $(k_x, k_y) = (1, 1)$ remains trapped in its initial configuration. Therefore, one may conclude that mode trapping and asymmetric mode power transfer are also exhibited by two-dimensional complex lattices.

VII. CONCLUSIONS

To conclude, based on the two-waves model, a theoretical study on the propagation of a wide beam through a transversal periodic photonic lattice described by a $\mathcal{PT}$-symmetric refractive index is developed, focusing on the behavior of power oscillations of a pair of resonant Bragg modes. As expected, within the paraxial wave approximation, a symmetry-breaking phase transition is obtained by varying a critical parameter β that measures the depart of the system from its Hermitian character. We have shown that small changes in this order parameter dramatically affect the dynamics and there are three regimes determined by β: for $\beta < \beta_c$ the beam power oscillates between the two modes; for $\beta > \beta_c$ it increases exponentially in a particular mode; while for $\beta = \beta_c$, depending on the initial condition, it remains constant or it grows as a quadratic function. Thus, we obtain power oscillations in the symmetric phase and biased mode trapping at the critical point. It should be noted here that the same behavior has been reported previously [24] as a universal behavior typical of phase transitions, due to the fact that microscopic details are not important. Therefore, the results found here should apply to a wide class of $\mathcal{PT}$ systems. To investigate the validity of the approximation, we have verified our results and their limitations by simulating the propagation of finite-width Gaussian pulses. Furthermore, extending the model to a two-dimensional wave equation, we have also observed power oscillations and power trapping. Although the results obtained here are based on a simple model, we have shown that they are exceptionally reliable. Due to its relative simplicity we hope that the present model might offer insights into the study of systems with generalized $\mathcal{PT}$ symmetries and an easy way for testing $\mathcal{PT}$ concepts. Considering the enormous potential of experimental researchers to produce artificial materials, one might conjecture that $\mathcal{PT}$-symmetric artificial systems should unravel a new generation of optical materials and, consequently, of optical devices.

[1] C. M. Bender and S. Boettcher, Phys. Rev. Lett. **80**, 5243 (1998).

[2] C. M. Bender, Rep. Prog. Phys. **70**, 947 (2007).

[3] C. M. Bender, D. C. Brody, and H. F. Jones, Phys. Rev. Lett. **89**, 270401 (2002).

[4] C. M. Bender, D. C. Brody, and H. F. Jones, Am. J. Phys. **71**, 1095 (2003).

[5] C. M. Bender, G. V. Dunne, and P. N. Meisinger, Phys. Lett. A **252**, 272 (1999).

[6] K. G. Makris, R. El-Ganainy, D. N. Christodoulides, and Z. H. Musslimani, Phys. Rev. A **81**, 063807 (2010).

[7] V. V. Konotop and B. I. Mantsyzov, Opt. Exp. **24**, 26146 (2016).

[8] M. V. Berry, J. Phys. A **41**, 244007 (2008).

[9] A. Ruschhaupt, F. Delgado, and J. G. Muga, J. Phys. A **38**, L171 (2005).

[10] K. G. Makris, R. El-Ganainy, D. N. Christodoulides, and Z. H. Musslimani, Phys. Rev. Lett. **100**, 103904 (2008).

[11] S. Klaiman, U. Günther, and N. Moiseyev, Phys. Rev. Lett. **101**, 080402 (2008).

[12] O. Bendix, R. Fleischmann, T. Kottos, and B. Shapiro, Phys. Rev. Lett. **103**, 030402 (2009).

[13] A. Guo, G. J. Salamo, D. Duchesne, R. Morandotti, M. Volatier-Ravat, V. Aimez, G. A. Siviloglou, and D. N. Christodoulides, Phys. Rev. Lett. **103**, 093902 (2009).

[14] S. Longhi, Phys. Rev. Lett. **103**, 123601 (2009).

[15] N. Bender, H. Li, F. M. Ellis, and T. Kottos, Phys. Rev. A **92**, 041803(R) (2015).

[16] Z. Lin, H. Ramezani, T. Eichelkraut, T. Kottos, H. Cao, and D. N. Christodoulides, Phys. Rev. Lett. **106**, 213901 (2011).

[17] C. E. Rüter, K. G. Makris, R. El-Ganainy, D. N. Christodoulides, M. Segev, and D. Kip, Nat. Phys. **6**, 192 (2010).

[18] A. Regensburger, C. Bersch, M. Miri, G. Onishchukov, D. N. Christodoulides, and U. Peschel, Nature (London) **488**, 167 (2012).

[19] V. S. Shchesnovich and S. Chávez-Cerda, Opt. Lett. **32**, 1920 (2007).

[20] P. A. Brandão and S. B. Cavalcanti, Opt. Commun. **400**, 34 (2017).

[21] S. Longhi, Phys. Rev. A **81**, 022102 (2010).

[22] E.-M. Graefe and H. F. Jones, Phys. Rev. A **84**, 013818 (2011).

[23] A. Yariv and P. Yeh, *Optical Waves in Crystals* (John Wiley and Sons, New York, 1984).

[24] M. C. Zheng, D. N. Christodoulides, R. Fleischmann, and T. Kottos, Phys. Rev. A **82**, 010103(R) (2010).